GEOPHYSICS, VOL. 71, NO. 1 (JANUARY-FEBRUARY 2006); P. B17–B27, 8 FIGS.
10.1190/1.2168007

Case History

Mapping 3D salt using the 2D marine magnetotelluric method: Case study from Gemini Prospect, Gulf of Mexico

Kerry W. Key[1], Steven C. Constable[1], and Chester J. Weiss[2]

ABSTRACT

The dominant salt body at Gemini Prospect, Gulf of Mexico, has been analyzed by seismic methods, revealing a complex 3D salt volume at depths 1 to 5 km beneath the mud line. Because of the high contrast in electrical conductivity between the salt and surrounding sediments, Gemini is an attractive target for electromagnetic interrogation. Using a broadband magnetotelluric (MT) sensor package developed at the Scripps Institution of Oceanography, data in the period band of 1 to 3000 s were collected at 42 sites in a series of profiles over Gemini, one of which was directly over a linear ridgelike salt feature striking roughly northwest–southeast and another orthogonal to it. These two profiles reveal that the strongest MT response arises when the electric field is oriented northeast–southwest.

We test the suitability of 2D inversion of these data for recovering the true salt structure by examining inversions of both actual data and synthetic 3D MT responses derived from the seismically inferred salt volume. Occam inversions of the northeast–southwest component result in resistivity images that generally agree with the seismic data, whereas inversions of the complementary component yield significantly poorer fidelity. Disagreement is greatest (1–2 km) along the salt sides and base. Depth errors for top of salt are less than 500 m. Although thin, deep salt (<1 km thick at 5 km depth) is not well resolved, the inversions reveal a resistive basement and a shallow subseabed environment rich in electrical heterogeneity that is weakly, if at all, suggested by the seismic data. A notable exception is a correlation between a previously uninterpreted seismic reflector and the base of a shallow resistivity anomaly whose presence is consistent with gas accumulation near the hydrate stability zone.

INTRODUCTION

Allochthonous salt structures such as those in the offshore northern Gulf of Mexico (Diegel et al., 1995; Peel et al., 1995; Schuster, 1995) play an important role in the deformation of sediments and subsequent formation of hydrocarbon reservoirs. Knowledge of the shape and extent of salt structures and their tectonic history is important when exploring for subsalt petroleum reservoirs. Reflection seismology, the primary technique for imaging crustal structures, can often provide detailed images of top- and base-of-salt surfaces, sedimentary layers, and basement formations. This level of detail can be used to construct a tectonic history and to infer where sediment layers have been deformed or juxtaposed to form potential traps for hydrocarbons. However, reflection data may not always provide sufficient detail to interpret salt and nearby sedimentary structures. Common problems associated with salt include multiple reflections and mode conversions (Ogilvie and Purnell, 1996), loss of reflected energy from steeply dipping salt surfaces, and lack of coherent features beneath salt structures. These problems give rise to unresolved salt boundaries on steeply dipping sides and bases of the salt and can result in interpretational ambiguities. These complications motivated research into a complementary technique for mapping salt structures: the marine magnetotelluric (MT) method. The large resistivity contrast between resistive salt

Manuscript received by the Editor April 2, 2004; revised manuscript received June 30, 2005; published online January 12, 2006.
[1]Scripps Institution of Oceanography, University of California San Diego, 9500 Gilman Drive, MC-0225 La Jolla, California 92093-0225. E-mail: kkey@ucsd.edu; sconstable@ucsd.edu.
[2]Sandia National Laboratories, Geophysics Department, P.O. Box 5800, MS-0750, Albuquerque, New Mexico 87185. E-mail: cjweiss@sandia.gov.

and relatively conductive porous sediments makes salt structures suitable targets for electrical methods.

Marine controlled-source electromagnetic (CSEM) methods are sensitive to thin, resistive structures (Eidesmo et al., 2002), but the presence of massive, resistive salt roots surrounded by relatively conductive sediments provides a better target for MT exploration (Hoversten and Unsworth, 1994). Despite limitations, MT surveys have an advantage over controlled-source methods when considering logistics and data acquisition costs because they do not require the deployment of a transmitter antenna, eliminating the costs of ship time for the transmitter antenna deep tow, the associated shipboard infrastructure, and added personnel costs for transmitter operations. MT techniques have been used effectively on land for petroleum exploration (Vozoff, 1972). However, early marine work was confined to very shallow water and was limited because of bulky equipment and wave noise (Hoehn and Warner, 1986). More recently, numerical model studies show that marine MT data in the period band of 1 to 1000 s are sensitive to salt geometry and can distinguish between shallow and deeply rooted salt structures (Hoversten et al., 1998). The amplitudes of such short-period electric and magnetic fields lie below the sensitivity threshold of traditional academic marine MT instruments, which were designed to respond to stronger-amplitude fields at periods greater than about 500 s (Filloux, 1987). A more recent approach to marine MT instrumentation has led to the development of a broadband marine MT instrument that measures both electric and magnetic fields from 0.1 to 10 000 s (Constable et al., 1998). The broadband instrument achieves this bandwidth through the combined use of ac-coupled sensors and high-gain, low-noise amplifiers, which allow measurement of smaller electric- and magnetic-field variations present at short periods (Key, 2003).

Little evidence suggests that marine electromagnetic methods will soon replace seismic techniques as the primary tool for oil and gas exploration. However, both marine MT and CSEM techniques have received increased attention (e.g., Hoversten et al., 2000; Eidesmo et al., 2002; Ellingsrud et al., 2002) for their potential to minimize uncertainty in reservoir detection and characterization (especially in deep water (>1 km) where drilling costs can exceed $10 million). In part, the value lies in the EM and seismic methods providing a complementary and largely independent map of the physiochemical state of the subseabed, which is evidenced through either its mechanical (detected by seismic methods) or its electrical properties (detected by MT/CSEM), each of which depends to some degree on geologic structure, lithology, fluids, and the porosity/permeability field. MT/CSEM data arise from the physics of diffusive energy transport, resulting in observations free from the analogous scattering and reverberation effects typical of high-fidelity wave propagation of seismic energy within saltbodies. Thus, the seismic characterization of structural boundaries can be augmented, or challenged, by the naturally occurring broad-spectrum MT signal (here, measured between 1 and 3000 s), itself strongly dependent on subseabed porosity and fluid type.

We investigate the effectiveness of using 2D marine MT methods to map 3D salt structures by presenting a case study of MT sites collected at the subsalt discovery at Gemini Prospect in the northern Gulf of Mexico. While we have seen large advances in 3D inversion techniques (e.g., Mackie and Madden, 1993; Newman and Alumbaugh, 2000), 2D inversions are faster to compute, allow for a finer model discretization, and are performed routinely — often as starting models for later 3D inversions. With those considerations, it is worthwhile to understand the practical limitations of 2D inversion when the structure is known to be three dimensional. At Gemini, top- and base-of-salt surfaces provided by an industry 3D seismic survey allow us to undertake such a controlled study. First, we use synthetic data inversions to estimate how well 2D inversion can recover sections of a known 3D model. Then, we apply the same inversion methodology to the real, or observed, MT data. Finally, we show that an improved interpretation is possible using both seismic and MT models in combined images of depth-migrated seismic reflection and inverted MT resistivity.

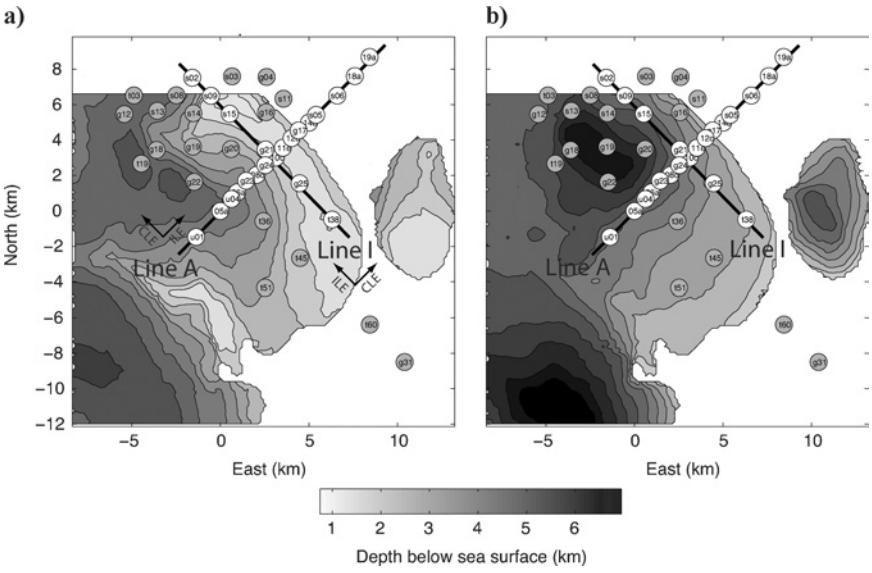

Figure 1. Gemini marine MT sites and salt structure. White circles show the locations of MT sites used in this paper. Gray circles show additional sites analyzed in Key (2003). Filled contours show the location of the (a) top-of-salt and (b) base-of-salt surfaces determined from an industry 3D seismic survey. The northern extent of the available salt-surface data ends abruptly at about 6.5 km north. Black lines show the two MT transects modeled in this paper.

GEMINI PROSPECT

Gemini Prospect lies about 200 km southeast of New Orleans in 1-km-deep water in the northern Gulf of Mexico. The Gemini salt structure is located on the eastern flank of a roho system (Schuster, 1995) that is about 16–24 km wide and 72 km long. Salt has been forced out both basinward and laterally, resulting in a complex 3D structure. Figure 1 shows the Gemini salt structure as determined from top- and base-of-salt picks from a commercial 3D seismic survey. Most of the salt lies between 1 and 5 km beneath the seafloor. The top-of-salt surface has a predominant northwest–southeast structural strike. The

base-of-salt surface has a basinlike shape with depths exceeding 6 km to the northwest. This deep portion of the base of salt is less well constrained, as the base-of-salt seismic reflections disappear here. There is some ambiguity as to whether the salt continues down to the evacuated Louann Salt source layer as a feeder stock or if the salt merely bottoms out at 6 km. Based on the lack of coherent reflections in a regional seismic profile, Schuster (1995) interprets this region as a possible salt feeder. The subsalt prospect at Gemini consists of a gas sand located at about 4 km depth on the southeastern edge of the Gemini salt structure (Ogilvie and Purnell, 1996).

MAGNETOTELLURIC SURVEYS

Gemini has been a test bed for developing the marine MT method for mapping base-of-salt depths (Hoversten et al., 2000) and for the continued improvement of the Scripps Institution of Oceanography broadband marine MT/EM instrument (Constable et al., 1998). Test deployments in 1997, 1998, 2001, and 2003 have resulted in 42 sites of MT data in the period band 1–3000 s at locations shown in Figure 1. A 2D inversion of the 1997 data showed that even with only a few data sites, MT methods can recover the base of salt to within 5% to 10% of burial depth (Hoversten et al., 2000). While this suggests success for the method, the 1997 data (nine sites from line *A* in Figure 1) were chosen to be most amenable to 2D modeling, as evident in the predominantly 2D strike of the top-of-salt surface, which raises the question as to whether the method can handle more complicated structural geometries.

To broaden the test of the marine MT method's ability to detect resistive salt, the following years' deployments were spread out across a wider region of the salt structure. Our paper expands the 2D analysis to include eight additional sites collected along line *A* and seven sites located along line *I* (Figure 1). Line *I* lies predominantly along the shallow top-of-salt ridge and crosses over a highly 3D region of the salt structure in the northwest, providing a suitable data set for assessing the ability of 2D inversion to map complicated 3D resistive structures. These and other transects of the 42 MT sites are presented in Key (2003).

MAGNETOTELLURIC DATA

During each survey, time series of the horizontal electric and magnetic fields were collected simultaneously at several sites for 1 to 2 days. The simultaneous recording of data at many sites allowed impedance tensor estimates to be calculated using a robust, multistation transfer-function estimation routine (Egbert, 1997). Experience with this routine has shown that a land remote-reference MT station is not necessarily required; land remote-reference stations were no longer occupied after the 1998 survey. Impedance-tensor estimates were calculated for each site over the period band of 1 to 3000 s. Seafloor orientations of the sensors were determined through a combination of mechanical or electronic compass readings from each deployment, along with analysis of interstation transfer tensors between electric and magnetic fields. Variability in the type of compass hardware and its integration into the sensor package required that orientation be handled on a case-by-case basis. Details of the procedure are documented by Key (2003).

Data quality is generally good but is also variable between the different survey years and sites for several reasons. Deployments at Gemini were usually done as tests of new instrument modifications before use on commercial surveys, so (the inevitable) problems were often discovered and fixed during these deployments. For example, electric and magnetic fields were recorded on separate instruments during the 1997 survey in an attempt to isolate and characterize instrument-motion noise recorded on the magnetic sensors. The magnetic-field instruments were outfitted with 200-kg concrete anchors (sea slabs) that greatly stabilized the instrument on the seafloor and improved data quality. After reducing motion noise by using sea-slab anchors, subsequent surveys recorded both electric and magnetic fields on one instrument. Source-field strength variations also affected data quality. A large magnetic storm occurred during the spring 2001 survey and resulted in high-quality data for all deployments. Conversely, weather and problems with ship equipment during the 2003 survey resulted in shorter deployments coincident with a period of relatively low source-field strength, yielding clean data only from 10 to 1000 s. At short periods where the overlying seawater greatly attenuates the MT source field (Constable et al., 1998; Key, 2003), variations in source-field strength resulted in some surveys acquiring data to periods as short as 1 s, while others yielded data good only to periods as short as 10 s.

An example of high-quality marine MT data collected at site s13 is shown in Figure 2. Site s13 is located over a thick, deep portion of the salt structure. The slight increase in apparent resistivity centered around 10 s is an example of the small MT response of the salt structure. Salt is very resistive (>10 Ω·m) compared to seawater (0.3 Ω·m) and seawater-saturated sediments such as those found at Gemini (around 0.5 Ω·m). Unlike the case of conductive targets that can

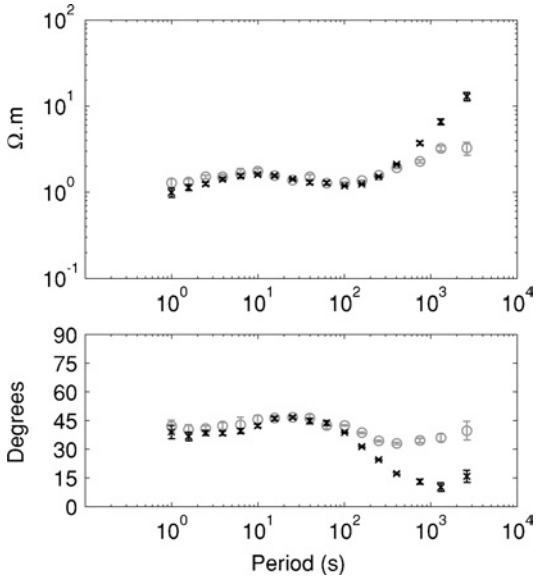

Figure 2. High-quality marine MT apparent-resistivity and phase data from site s13, which is located over a thick portion of the salt. Black symbols are for the off-diagonal impedance component with the electric field oriented to the southeast; gray symbols are for the electric field oriented to the northeast.

generate large secondary fields and strong MT responses, the resistive salt forces induced currents to flow around rather than through it and yields only minor secondary fields and very small MT responses. The MT response effectively saturates after the first factor of 10 or so in resistivity contrast and results in seafloor impedances more sensitive to the shape of the salt body than the absolute resistivity. At periods longer than 250 s, the apparent-resistivity and phase curves separate for each electric-field polarization. At these long periods the MT skin depth (*e*-folding distance of the EM fields) becomes much greater than the base-of-salt depths, indicating that the split in the MT responses is probably caused by a deep 2D or 3D structure and/or the conductivity contrast associated with the nearby continental shelf seafloor topography (Key, 2003). To minimize these potential 3D effects from contaminating the 2D inversion models, only MT responses at periods up to 250 s were analyzed for the modeling section of this paper.

The top rows of Figures 3–6 show MT response pseudosections from 1 to 250 s for lines *A* and *I*. The responses are for the off-diagonal impedance components that correspond to horizontal electric fields oriented either along the line (in-line electric, or ILE) or across the line (cross-line electric, or CLE), as referenced to the azimuth of each line. Specifically, line *A*'s responses correspond to southwest–northeast (ILE) and southeast–northwest (CLE) directed horizontal electric fields. For line *I* the directions are reversed: ILE and CLE responses correspond to southeast–northwest and southwest–northeast horizontal electric fields, respectively. To accentuate the subtle features of the data, the apparent resistivities and phases are shown on a linear color scale. The pseudosections exhibit no large static shifts in the data, although there are examples of along-line variability in MT response (such as neighboring stations 10c and g21 in Line *I*) which should not be confused with static shifts as commonly defined in the MT literature (e.g., Sternberg et al., 1988). The line *A* ILE pseudosection (Figure 3) shows more structure than the CLE pseudosection (Figure 4). The ILE pseudosection shows higher apparent resistivities and lower phases at sites located above the shallowest portions of the salt, with apparent resistivities of up to 1.4 Ω·m and phases as low as 30°. The low phases, indicative of salt, appear at shorter periods than the corresponding apparent-resistivity increase. For line *I*, the CLE pseudosection (Figure 6) shows more structure than the ILE pseudosection (Figure 5). With the exception of site s02, the CLE apparent resistivities increase from about 0.5 to 1.2 Ω·m as the period increases, and the CLE phases show a local minimum at periods of 10 to 100 s. Both features are much less pronounced for the ILE pseudosections.

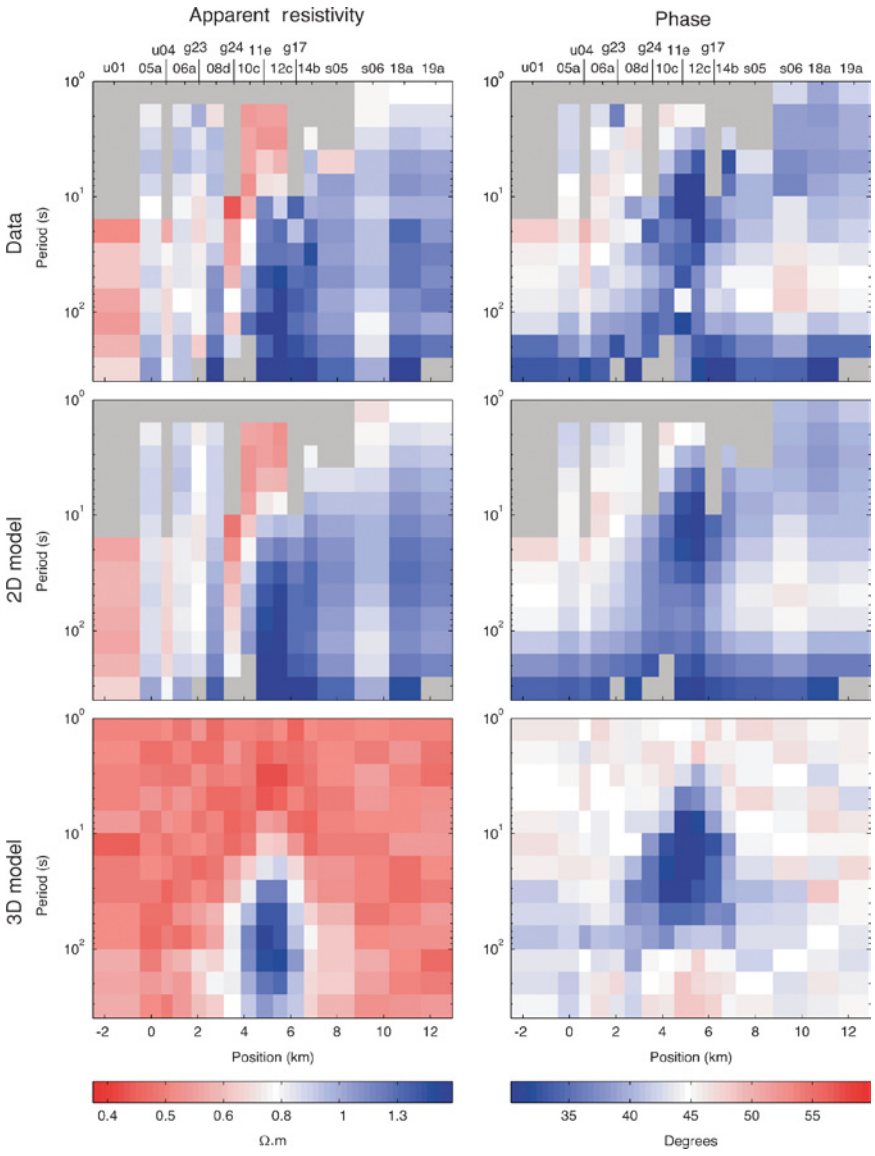

Figure 3. Line *A* pseudosections for the off-diagonal impedance component corresponding to the in-line electric field (i.e., oriented 45° east of north). Apparent resistivity (left column) and phase (right column) are shown for the observed data (top row), 2D inversion model response (middle row), and the 3D seismic salt volume forward response (bottom row). Gray areas correspond to regions of unusable data. Apparent resistivity and phase are shown on a linear color scale.

Previous analysis of a subset of line *A* data using polar impedance diagrams (Hoversten et al., 2000, their Figure 8) clearly identifies the period bands in which the observations are dominated by shallow 1D layering (<20 s), by the deeper 2D top-of-salt ridge (20–250 s), and by the full 3D structure of the salt body, surrounding basement, and regional bathymetry (>250 s). Although not shown, similar 1D to weakly 2D polar diagrams occur at 1 to 250 s for the additional sites considered here, suggesting that 2D inversions should adequately resolve any local 2D structure beneath the lines.

MODELING

The modeling section of this study consists of two components. For the first part, synthetic data inversions were conducted by computing 3D MT responses for the seismic salt structure and then inverting the responses using a 2D algorithm. In the second part, the same 2D inversion procedure was applied to the real Gemini MT data. The differences between the synthetic-data inversion models and the seismic salt structure help us calibrate how well 2D inversion recovers the salt and also provide a basis for comparison with the real-data inversions.

Lines *A* and *I* are perpendicular to each other and present some potential problems for traditional 2D interpretation. One complexity is the concept of geoelectric strike direction. In a general 2D analysis, there exists a strike direction in which conductivity is invariant at least on some scale length appropriate for the conductivity and frequencies of interest such that 2D modeling is physically accurate. The prominent northwest–southeast-striking ridge in the top of salt suggests that line *A* meets this requirement; indeed, 2D inversions of the 1997 MT data (Hoversten et al., 2000) recovered the salt, despite the high 3D curvature of the base of salt. For line *I*, traditional 2D interpretation seems unjustified since it lies along the same shallow axis of the top of salt that was used for the strike of line *A* and also crosses highly 3D regions of the salt to the north. However, both lines have low phase-sensitive skew values and only a moderate amount of structure in the pseudosections, suggesting that a 3D model might not be required to fit the data. Although 1D modeling might adequately fit individual components of the observed data, we opted instead for 2D inversion since the integrating power of regularization would allow correlated data features in adjacent sites to be incorporated into the final model, despite site-to-site variations in noise.

The effectiveness and potential pitfalls of 2D inversion for known 3D environments have been studied for a range of problems (e.g., Hoversten et al., 1998; Ledo et al., 2002; Siripunvaraporn et al., 2005), yet no general rule of thumb for successful 2D inversion exists. For intersecting MT transects, Park and Mackie (2000) suggest an iterative process of 2D inversion and 3D forward modeling to effectively identify and omit subsets of data most sensitive to 3D features. In their study of a heterogeneous region of highly variable resistivity (over three orders of magnitude variation), 3D effects were determined on a site-by-site basis and found to be largest at long periods (for certain sites) and to vary between the impedance components. As stated previously, in our analysis we omit data at periods greater than 250 s, where the influences of regional bathymetry and deep basement formations add complexity. We also expect 3D effects to be less substantial than in Park and Mackie (2000) because of the subtleness of the Gemini MT responses. We start our analysis by using synthetic-data inversions to identify which subset of the data (ILE or CLE) best recovers the salt intrusion beneath each line.

2D inversion of synthetic 3D forward data

The model study was performed by creating synthetic 3D MT data for both lines using the seismic salt model, adding a small amount of random noise to the data, and then using 2D inversion to attempt to recover and image the salt underneath each line. The 3D MT forward response of the

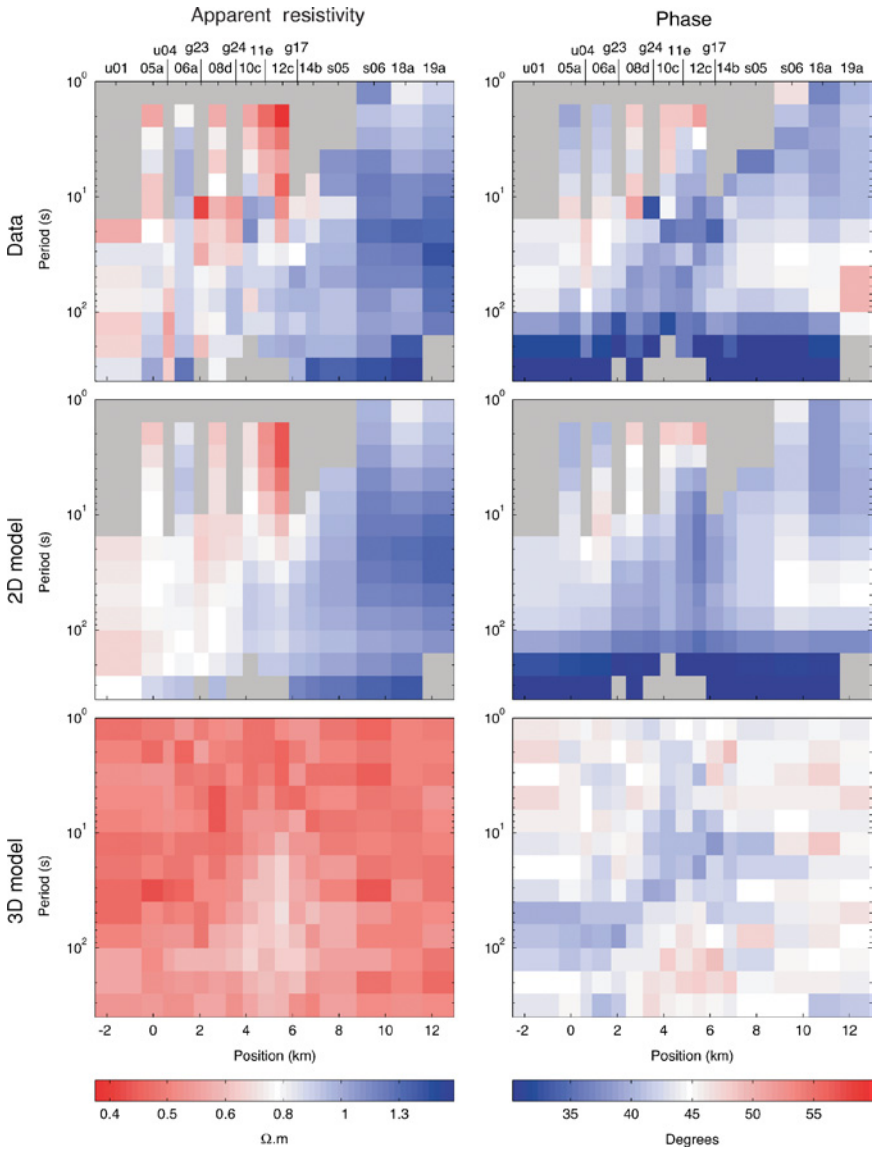

Figure 4. Line *A* pseudosections for the off-diagonal impedance component corresponding to the cross-line electric field (i.e., the electric field oriented 45° west of north). See Figure 3 caption for details.

salt body was computed using a variation of a staggered-grid, finite-difference formulation (Newman and Alumbaugh, 1995), written to use a matrix-free approach (Weiss, 2001) to reduce computational storage requirements. The finite difference mesh was designed by dividing the survey region into cells 350 × 350 m wide horizontally and 100 m thick vertically, resulting in a 113 × 112 × 111 node grid. Resistivities within the salt region were set to a uniform value of 100 Ω·m. Resistivity values outside the salt were set to 0.5 Ω·m, a value commensurate with the real-data 2D inversion results and equivalent to porous marine sediments saturated with seawater. A 1000-m-thick seawater layer of 0.3 Ω·m was added to the model to satisfy the seafloor boundary condition, which allows vertical electric current at the seafloor-sediment interface (Hoversten et al., 1998). MT forward responses were calculated for the same site locations and frequencies used for the real data. The synthetic forward-response data were contaminated with 5% random Gaussian noise added to mimic the errors present in the observed data (Constable, 1991). Data generated from this process are referred to as synthetic data (bottom row, Figures 3–6). The synthetic data reproduce many features of the real data yet contain much less variability. Some of the differences may be attributed to noisy real-data points, but most of the differences are probably from additional heterogeneity at Gemini absent in the simple, uniform salt-and-sediment 3D model.

The 2D models were computed from the synthetic data using the regularized Occam 2D MT inversion (Constable et al., 1987; deGroot-Hedlin and Constable, 1990), which utilizes a finite-element code (Wannamaker et al., 1987) to compute the model's forward response and Jacobian matrix. The inversion regularization consisted of a roughness penalty applied to resistivity variations between both horizontally and vertically adjacent model blocks (deGroot-Hedlin and Constable, 1990). Although recent inversion techniques have concentrated on sharp boundaries or contrasts in model structure to be consistent with structures having well-defined geologic boundaries (Smith et al., 1999; Mehanee and Zhdanov, 2002; deGroot-Hedlin and Constable, 2004), we used smooth inversion to find models with the minimum amount of structure required by the MT data. While a sharp boundary model for line *A* agrees better with the seismically determined salt model (Hoversten et al., 2000; deGroot-Hedlin and Constable, 2004), smooth models illuminate only those structures that significantly affect the data and thus reflect more the resolution power of marine MT.

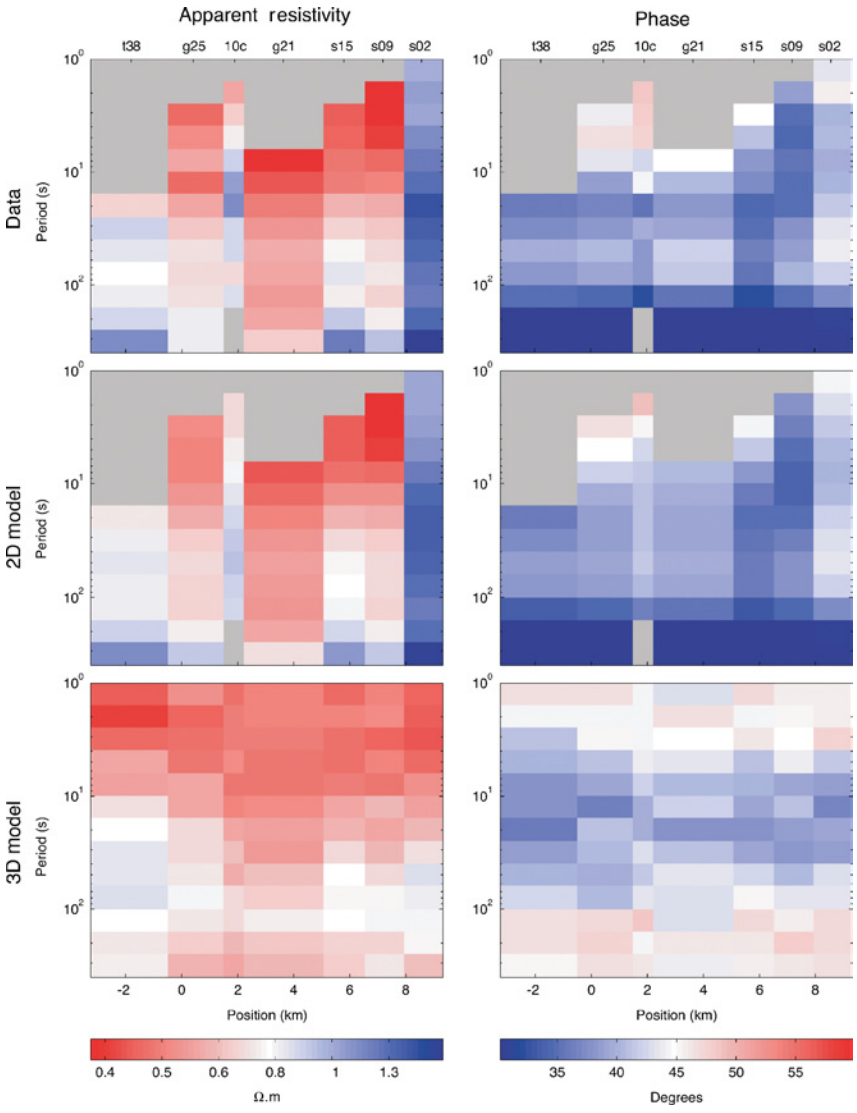

Figure 5. Line *I* pseudosections for the off-diagonal impedance component corresponding to the in-line electric field (i.e., the electric field oriented 45° west of north). See Figure 3 caption for details.

For a 2D structure, Maxwell's equations decouple, allowing for the option of inverting each off-diagonal component of the 2 × 2 impedance tensor separately. One off-diagonal component corresponds to electric currents flowing parallel to the direction of conductivity invariance (the TE mode for 2D environments), and the other corresponds to currents flowing perpendicular to this direction (TM mode). For truly 2D situations, modeling both components provides a maximum constraint on model structure. For elongated 3D conductive features, modeling the impedance component with the electric currents flowing perpendicular to the conductivity invariant direction is generally considered to be more accurate since it includes the effects of boundary charges on lateral conductivity variations (Wannamaker et al., 1984). Numeric modeling of a 3D salt anticline also suggests this result (Hoversten et al., 1998). However, both of these studies contain conductive features (the core of the salt anticline was a region of conductive sediments) and do not necessarily apply to the resistive salt at Gemini, which essentially occludes electric currents. To investigate which component would recover the salt best, we inverted

each off-diagonal impedance component separately. Our mapping of impedances from the data domain to the model domain was straightforward: ILE impedances were inverted for the case of electric fields perpendicular to the direction of assumed conductivity invariance, and CLE impedances were inverted for the case of electric fields parallel to this direction. The models computed by these synthetic inversions are shown in the right-hand columns of Figures 7 for (a) line *A* and (b) line *I*. Each inversion used a model consisting of about 2200 unknown parameters and a 1-Ω·m half-space starting model. All inversions easily achieved an rms misfit of 1.0 and used a uniform data error of 5%.

The recovered inversion models for a given line show substantial differences in structure between the two inverted impedance components. Both the line *A* ILE and the line *I* CLE inversions resolve the salt as resistive anomalies of about 2 to 10 Ω·m, while the line *A* CLE and the line *I* ILE inversion models only show hints of resistive features where the salt is shallowest. For the line *A* ILE and the line *I* CLE inversions, the saturation effect in the MT responses discussed earlier results in the inversion recovering the salt as resistivity values much less than the 100-Ω·m forward-model value. Using 1.5 Ω·m as the boundary between salt and sediments, the line *A* ILE inversion shows good agreement with the top-of-salt boundary that is shallower than 4 km. The base of salt is less well resolved and is overestimated by up to 1 km in depth and 2 km in lateral position. Where the salt is thinnest and deepest along the left portion of the model, no resistive structure is imaged. The CLE inversion for line *I* generally shows a resistive structure where the model contains salt. However, the base-of-salt depths are overestimated by up to 2 km on the left side of the model and underestimated by about 1 km on the right side. The lateral extent of the resistive feature is about 2 km short of the salt edge on the left side and about 2 km too long on the right.

The disagreement between the 2D inversion models and the seismic salt boundaries deserves several comments. The lack of resolution of the thin and deeply buried salt is no surprise since modeling studies show this (Hoversten et al., 1998) and MT method in general is ineffective in detecting thin resistors. Where resistive features are resolved, the lateral and vertical differences are probably attributable to a few causes. For both lines, 2D inversions of synthetic 3D data without the 5% random noise added yield nearly identical models and suggest that noise is not causing the structural misfit. Although line *I* may have benefited from more MT sites, the number of MT observation sites above the salt on line *A* rules out insufficient measurements as the cause of the base-of-salt disagreement. Some portion of the boundary errors is most likely the result of the 2D inversion being corrupted by minor 3D effects in the MT responses. For instance, the overextending resistor on the right side of line *I* may occur because of 3D effects from the abrupt edge of the salt in the 3D model. The smooth regularization used in the inversion may also be smearing model structure where it is poorly constrained by the data. In summary, 2D inversion of 3D resistive salt can recover the general location of the salt when inverting the impedance component with the most structure; but the boundary locations can be off by 1 to 2 km, and thin and deep salt structures are not resolved.

2D inversion of real MT data

The observed MT data were inverted using the same inversion method and model design as for the synthetic data. The data-error floor was set to 5% in resistivity and 1.5° in phase

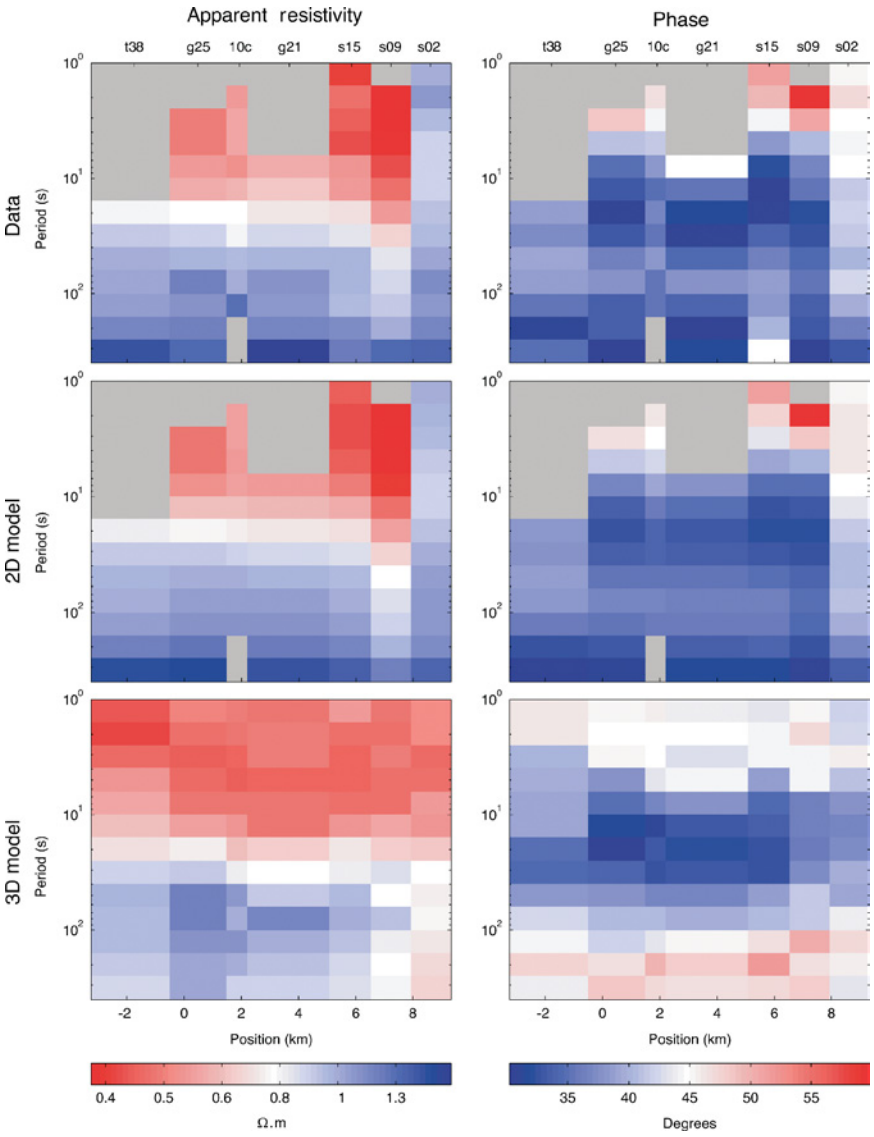

Figure 6. Line *I* pseudosections for the off-diagonal impedance component corresponding to the cross-line electric field (i.e., the electric field oriented 45° east of north). See Figure 3 for details.

(i.e., all errors <5% were set to 5%). The resulting models are shown in the left columns of Figure 7. For line *A*, the ILE and CLE models were fit to an rms misfit of 1.10 and 1.69, respectively; the CLE inversion had difficulty finding a model with a lower misfit without including some grossly irregular and obviously overfit structure. So this inversion was set to converge to a misfit of 1.69 instead of 1.0. The model responses (middle rows, Figures 3–6) capture most of the features observed in the real MT data, indicating a robust fit.

Both the ILE and CLE real-data inversions contain significantly more structure than the synthetic-data inversions. However, like the synthetic-data inversions, one impedance component resolves the salt structure better than the other. Both the line *A* ILE and the line *I* CLE inversion show the largest amount of structure that correlates with the seismic salt boundaries. The real-data inversions show an increase in resistivity at 6 to 8 km depth that is associated with a basement formation, a feature not included in the synthetic 3D model. Both line *A* inversions contain slightly resistive features between the salt and the basement. These are probably artifacts of the inversion regularization oversmoothing structure into regions that are not as well constrained by the data. In this case, the resistivity between the salt and basement represents the maximum value permissible without an increase in the data misfit.

Using 1.5 Ω·m as a salt boundary again, comparisons between the seismic salt, the real-data inversion, and the synthetic-data inversion can be made. The line *A* ILE inversion agrees well with the top-of-salt boundary, as is the case for the synthetic-data inversion. The real-data inversion agrees better with the lateral extent of the base of salt than the synthetic-data inversion does but does not agree as well with the depth extent since the resistive boundary is smeared into the basement. There is also an indication of shallow resistive features in both the ILE and CLE inversions for line *A*. The structure on the right side of the model is evident in the data pseudosections as consistently high apparent resistivities and low phases for sites s05 to 19a; neither feature is observed in the synthetic 3D data. The line *I* CLE inversion results from both the real and the synthetic data agree better with the salt boundaries than the ILE inversion. However, the real-data inversion has a shallow overhanging resistive region in the right side of the model that was not recovered by the synthetic data. This feature is located just past the northern boundary of the available seismic salt data and so was not included in the synthetic 3D MT model. The overhanging resistive feature in this region is probably a real aspect of the Gemini salt structure.

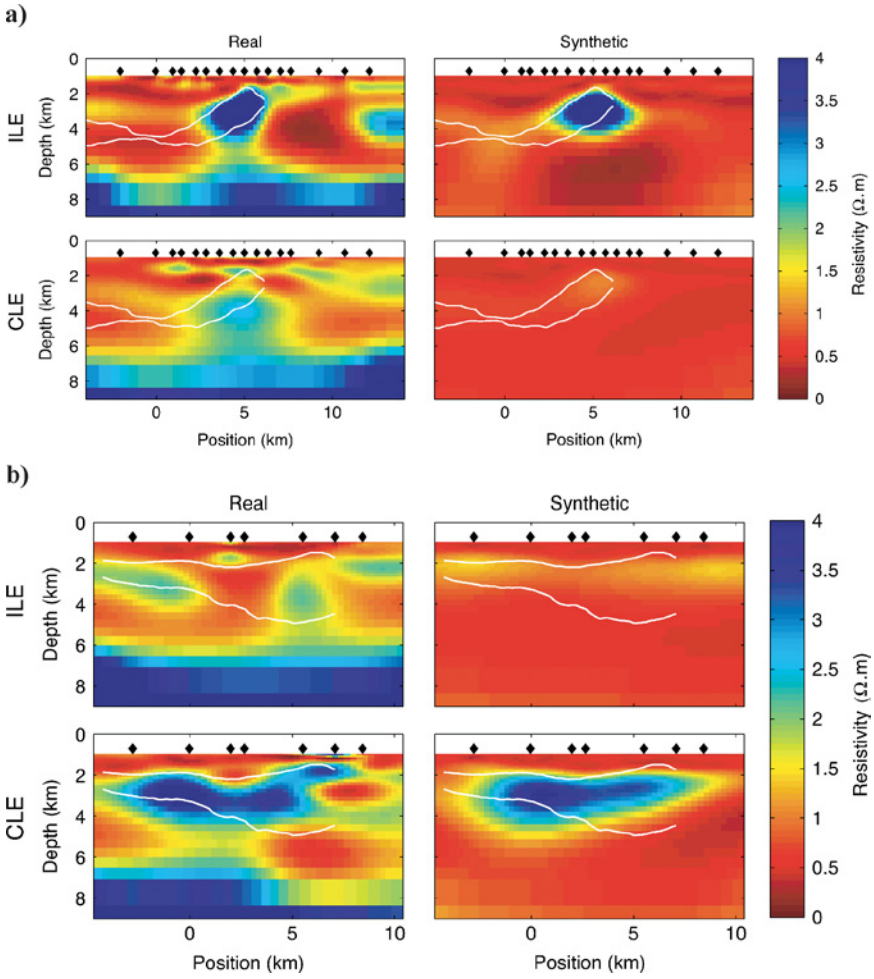

Figure 7. Inversion results for (a) line *A* and (b) line *I*. Real data are used for the figures on the left and synthetic 3D forward data for the figures on the right. The models are oriented from southwest (left) to northeast (right). The top and bottom rows show results for inverting the ILE and CLE impedance components, respectively. The white outline shows the location of the top and bottom surfaces of the salt structure as determined from 3D seismic reflection data. MT site locations are shown as black diamonds.

DISCUSSION OF MODELING RESULTS

The inversion results derived from the synthetic data demonstrate that the methodology used here is indeed conservative in its placement of electrical structure within the final model. There is a clear resistor in the vicinity of the seismically derived salt volume and virtually no structure elsewhere. Top-of-salt positions are generally well resolved and have errors in depth usually less than 500 m. Small 3D corrupting effects are present in some of the inversions, particularly the line *I* CLE synthetic data inversion, and result in base-of-salt and lateral-boundary-position errors of 1 to 2 km. However, the synthetic study shows an important result: Both the CLE and ILE data can be modeled separately, and any resistive structure that does appear probably has basal and lateral boundaries accurate to within 1 to 2 km and top-of-salt boundaries accurate to within 500 m. This is also observed for other Gemini synthetic-data inversion profiles considered in Key (2003). A caveat is that deeply buried, thin, or highly narrow salt is usually not imaged, so it is

possible that any inversion model could also contain such unresolved structures. Although not presented here, we also tried inverting both the ILE and CLE data simultaneously. These inversions had more difficulty finding a low misfit, and the resulting models have spurious structures that do not conform to the salt boundaries. We interpret this as in indication that 3D effects substantially corrupt models obtained from 2D inversion of both ILE and CLE data but are less corrupting when inverting either data set alone. Thus, a full 3D inversion is probably required to obtain reasonable model features when inverting all of the data.

The real and synthetic data inversions share many features. Both recover broad resistive features in the general location of the seismic salt but only for the inversions of the off-diagonal impedance component with the largest amount of structure in the pseudosections. For example, the line *A* ILE data show more variability than the CLE data; hence, the ILE inversion best reproduces the salt. Line *I* shows a similar result but for the CLE data and inversion. In general, the impedance component associated with horizontal electric currents flowing along a southwest–northeast path agree best with the known structure.

Considering only the line *A* ILE and the line *I* CLE inversions, the resolved portions of the salt reside at subseafloor depths of less than 4 km and are relatively thick compared to the depth extent. Although numerical modeling shows 2D inversion can recover some deep sill-shaped regions of salt (Hoversten et al., 1998), the lateral extent of salt at Gemini is limited, so none of the deep and thin salt along the left portion of line *A* was imaged. In this region, the inversion's regularization constraint smoothes the surrounding conductive region across the salt boundaries with little effect on the model's data fit. MT readings are preferentially sensitive to conductors, so the conductive regions that underlie the salt are much better constrained. These features indicate the salt is not rooted into the basement formation on either profile.

JOINT ANALYSIS WITH SEISMIC REFLECTION DATA

The preceding sections have shown that 2D MT can be effective for imaging certain salt structures; it is worthwhile to examine other features of the resistivity model. To do so, we present a joint analysis of seismic reflection profiles and MT inversions. Depth-migrated seismic reflection profiles were provided for lines *A* and *I* by WesternGeco and ChevronTexaco (David Bartel, personal communication, 2003). The inversions that showed the greatest amount of structure, the line *A* ILE and the line *I* CLE, were combined with the seismic profiles to create a model of both resistivity and seismic reflections (Figure 8).

The top-of-sait and base-of-salt reflections are readily apparent in Figure 8a because they are the strongest reflections at depths less than 6 km. As shown earlier, the MT model agrees well with the salt structure where it is shallower than about 4 to 5 km. Bright reflections seen at depths of about 7 km correspond with an increase in resistivity and show the transition to either basement rocks or an overlying chalk layer (Schuster, 1995). An increase in resistivity to about 1.5 Ω·m at depths of about 2 km and horizontal positions of about 6 to 10 km correlates well with some layering in the reflections. There is also an indication that this feature continues farther to the right of the model. A thin, resistive feature in this region is also required by controlled-source EM data collected on the 2003 cruise (J. Behrens, personal communication, 2003). This feature lies outside the seismically inferred salt and is probably not salt. This feature abuts the Gemini salt body along the lateral boundary of a regional roho system (Schuster, 1995), and there may be a component of strike-slip to the roho system along this edge.

Given this information, a few explanations are possible for the increase in resistivity. One is that the resistive feature represents a less porous and less permeable sedimentary layer which has a higher resistivity since it contains less seawater than the surrounding sediments. The layer may have once been continuous to the left portion of the model, but the listric growth faulting of the roho system and the salt intrusion has since rotated and displaced this layer basinward. Another

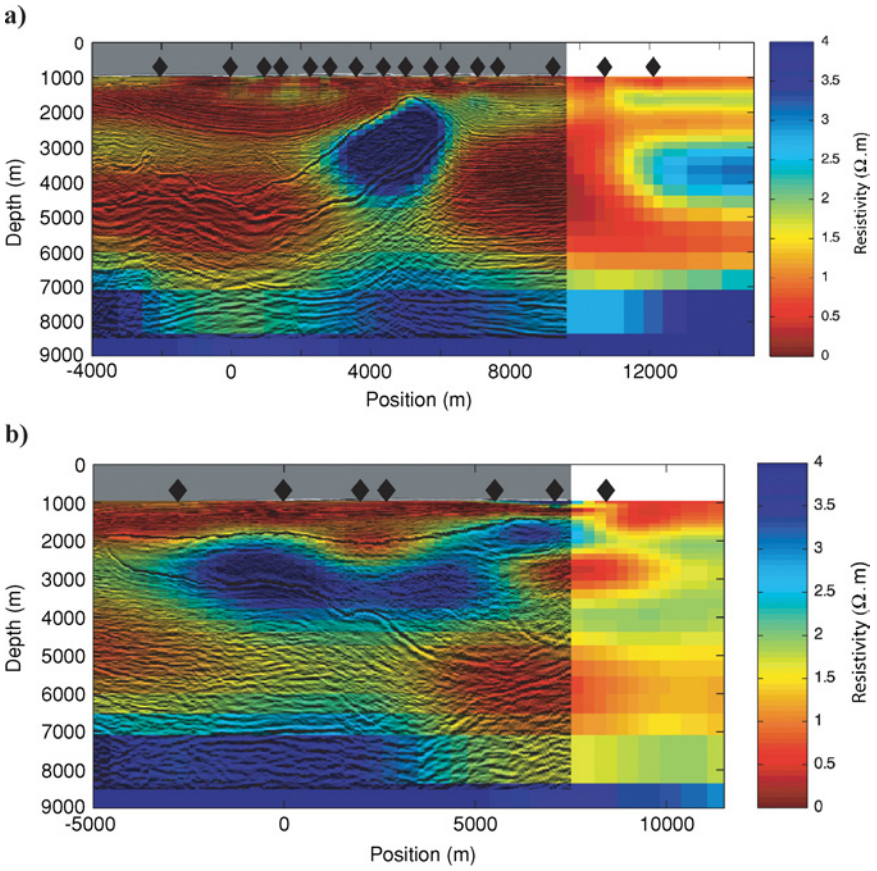

Figure 8. (a) Line *A* combined MT and reflection models. Black lines show depth-migrated reflections from a 3D seismic survey. (b) Line *I* combined MT and reflection models. Black lines show depth-migration reflections from a 3D seismic survey.

explanation is that the increase in resistivity represents an increase in pore-fluid resistivity. Resistive fluids in this layer may be contained by a natural trap formed by the salt intrusion and faulting, as shown by the seismic reflections bending up against the salt. If the resistive fluids are less dense than seawater, then they may have migrated laterally along the sloping sedimentary layers and become trapped by the relatively impermeable salt. The fluid may be a hydrocarbon, as it would then meet the requirement of being more resistive than seawater and less dense. The subsalt prospect at Gemini is a gas sand at about 4 km depth (Ogilvie and Purnell, 1996), so this shallower resistive feature may be an undetected gas accumulation. The depth of this feature straddles the gas hydrate stability zone for this region, depending on the methane content (Milkov and Sassen, 2000), so the resistor could indicate either gas hydrates or an accumulation of free gas abutting the base of the gas hydrate stability zone. A preliminary analysis of the controlled-source EM data along this line indicates the increase in resistivity is substantial (J. Behrens, personal communication, 2003), which suggests shallow gas or hydrate rather than a more subtle change in sediment or fluid conductivity.

The combined image for line *I* shown in Figure 8b illustrates how MT can help resolve structures in regions where seismic models are ambiguous. While the top-of-salt reflection is easily seen, the base-of-salt reflection loses coherence at lateral positions of about 5 km. The resistivity model helps resolve this ambiguity by suggesting that the salt is not deeply rooted in this region, as indicated by the low resistivity at depths of about 5 to 7 km. A shallow, thin finger of salt seen as a resistive feature at positions of about 5 to 8 km and depths around 2 km also correlates well with the top-of-salt reflection and is bound on the bottom by a reflection at about 2.5 km. As shown in Figure 7b, the interpreted base of salt from the seismic survey lies much deeper than this overhanging feature. The MT model contradicts this by indicating that the salt finger overhangs a conductive zone that is probably porous sediments. Beneath the conductive zone the resistivity increases slightly at depths of about 3.5 to 4.5 km but then decreases again at depths greater than about 4.5 km, indicating the salt does not have a resistive root here.

CONCLUSIONS

This study illustrates how the 2D marine MT method can be used to map portions of 3D salt. Gemini MT response pseudosections show varying degrees of structural sensitivity, depending on the direction of the corresponding horizontal electric field used to formulate the response. Independent inversions of each off-diagonal impedance component show that the data with the most pseudosection structure, generally the impedance component corresponding to a northeast–southwest electric field, agrees best with the known salt boundaries. Inversions of both off-diagonal impedance components yield highly irregular models, implying that the corrupting effects of 3D structures are most significant then and that a full 3D inversion is required to fit all data with a realistic model. For the independent inversions, we find lateral and bottom boundary errors of up to 1 to 2 km and top-of-salt boundary errors of up to 500 m. For both lines, salt shallower than about 4 to 5 km was imaged, but deep and highly 3D regions of the salt were not recovered. While thin, deep salt structures are beyond the sensitivity of marine MT data, thick and deep 3D regions of salt may be resolved in future 3D inversions that utilize the entire MT data set (including periods greater than 250 s).

We use minimum structure smoothing in our inversions to recover the simplest model required by the data. The stability of the smooth inversion allows robust 2D model features, constrained by the various data subsets (ILE, CLE, real, and synthetic), to be compared for accuracy with the true seismic salt beneath each profile. However, many improvements in the fidelity of the 2D inversions are possible. As mentioned, sharp boundary inversion techniques allow for more realistic abrupt resistivity contrasts and can increase the accuracy of the base-of-salt depths. However, sharp boundary methods have less flexibility than smooth inversions and can often get trapped in local minima, unnecessarily complicating assessment of 2D inversions. As with all inverse methods, incorporating additional a priori geologic information such as well logs or known geologic boundaries such as top of salt would further increase the accuracy of the final model. Including a higher density of sites would provide some improvement, particularly along line *I*, but would probably be very limited since the MT anomalies are quite small and for the most part do not vary to any great extent spatially (except between sites s09 and s02). The insensitivity of MT to thin, deep resistive layers can also be exploited to place an upper bound on the layer thickness, which remains undetectable until reaching a threshold thickness.

The joint presentation of seismic reflection and electrical resistivity allows a more complete interpretation of both data sets and supports stronger conclusions about the salt structure and surrounding sediments. Ambiguities in the seismic interpretation, particularly in regions where base-of-salt reflections are incoherent, can be resolved through such a joint interpretation. As practical 3D inversion of MT data becomes more commonplace (aided most substantively by Moore's law, perhaps), we believe preliminary 2D inversion can remain worthwhile because it is quicker, allowing data quality to be assessed and error floors to be set appropriately; it offers an improved starting model for 3D inversion; and it shows where the 3D inversion mesh needs to allow structure to develop. While future 3D inversions may more accurately determine salt boundaries, 2D inversion will remain a quick and easy tool for testing various hypotheses for salt structures and the surrounding sediments.

ACKNOWLEDGMENTS

K. Key acknowledges support from the Gerald W. Hohmann Memorial Scholarship. The Seafloor Electromagnetic Methods Consortium at Scripps Institution of Oceanography provided funding for this work. The authors thank David Bartel, ChevronTexaco, and WesternGeco for providing the 3D seismic data and salt volume; Arnold Orange and AOA Geophysics for their collaboration in collecting the MT data and support in developing the marine MT technology; the captains and crews of the *R/V Pelican, R/V Gyre*, and *R/V Longhorn*; and the following people for their efforts in the research cruises: Jacques Lemire, David Willoughby, Lisl and Rhodri Lewis, Ransom Reddig, Marianne Mulrey, Almuth von den Steinen, Adam Agundes, James Behrens,

Mark Everett, Joshua King, Lucy MacGregor, Hiatt Sheller, Cristiano Signorini, and Stephanie Rothe. James Behrens provided preliminary interpretations of the 2003 CSEM data. Gary Egbert and Phil Wannamaker are thanked for making their MT computer codes freely available. Assistant editor George Jiracek, associate editor Randy Mackie, and three anonymous reviewers provided useful suggestions for improving the quality of this paper. Sections of this work were performed at Sandia National Laboratories. Sandia is a multiprogram laboratory operated by Sandia Corporation, a Lockheed Martin Company, for the United States Department of Energy's National Nuclear Security Administration under contract DE-AC04-94AL85000.

REFERENCES

Constable, S., 1991, Comment on "Magnetic appraisal using simulated annealing" by S. E. Dosso and D. W. Oldenburg: Geophysical Journal International, **106**, 387–388.

Constable, S. C., R. L. Parker, and C. G. Constable, 1987, Occam's inversion — A practical algorithm for generating smooth models from electromagnetic sounding data: Geophysics, **52**, 289–300.

Constable, S. C., A. S. Orange, G. M. Hoversten, and H. F. Morrison, 1998, Marine magnetotellurics for petroleum exploration, part I: A sea-floor equipment system: Geophysics, **63**, 816–825.

deGroot-Hedlin, C., and S. Constable, 1990, Occam's inversion to generate smooth two-dimensional models from magnetotelluric data: Geophysics, **55**, 1613–1624.

———, 2004, Inversion of magnetotelluric data for 2D structure with sharp resistivity contrasts: Geophysics, **69**, 78–86.

Diegel, F. A., J. F. Karlo, D. C. Schuster, R. C. Shoup, and P. R. Tauvers, 1995, Cenozoic structural evolution and tectonostratigraphic framework of the northern Gulf Coast continental margin, *in* M. P. A. Jackson, D. G. Roberts, and S. Snelson, eds., Salt tectonics: A global perspective: AAPG Memoir 65, 109–151.

Egbert, G. D., 1997, Robust multiple-station magnetotelluric data processing: Geophysical Journal International, **130**, 475–496.

Eidesmo, T., S. Ellingsrud, L. MacGregor, S. Constable, M. Sinha, S. Johansen, F. Kong, and H. Westerdahl, 2002, Sea bed logging (SBL), a new method for remote and direct identification of hydrocarbon filled layers in deepwater areas: First Break, **20**, 144–152.

Ellingsrud, S., T. Eidesmo, S. Johansen, M. Sinha, L. MacGregor, and S. Constable, 2002, Remote sensing of hydrocarbon layers by seabed logging (SBL): Results from a cruise offshore Angola: The Leading Edge, **21**, 972–982.

Filloux, J. H., 1987, Instrumentation and experimental methods for oceanic studies, *in* J. Jacobs, ed., Geomagnetism: Academic Press, 143–248.

Hoehn, G. L., and B. N. Warner, 1986, Magnetotelluric measurements in the Gulf of Mexico at 20 m ocean depths, *in* K. Vozoff, ed., Magnetotelluric methods: Society of Exploration Geophysicists, 578–597.

Hoversten, G. M., and M. Unsworth, 1994, Subsalt imaging via seaborne electromagnetics: Proceedings of the Offshore Technology Conference, **26**, 231–240.

Hoversten, G. M., S. C. Constable, and H. F. Morrison, 2000, Marine magnetotellurics for base-of-salt mapping: Gulf of Mexico field test at the Gemini structure: Geophysics, **65**, 1476–1488.

Hoversten, G. M., H. F. Morrison, and S. C. Constable, 1998, Marine magnetotellurics for petroleum exploration, part II: Numerical analysis of subsalt resolution: Geophysics, **63**, 826–840.

Key, K., 2003, Application of broadband marine magnetotelluric exploration to a 3D salt structure and a fast spreading ridge: Ph.D. thesis, University of California, San Diego.

Ledo, J., P. Queralt, A. Marti, and A. G. Jones, 2002, Two-dimensional interpretation of three-dimensional magnetotelluric data: An example of limitations and resolution: Geophysical Journal International, **150**, 127–139.

Mackie, R. L., and T. R. Madden, 1993, Three-dimensional magnetotelluric inversion using conjugate gradients: Geophysical Journal International, **115**, 215–229.

Mehanee, S., and M. Zhdanov, 2002, Two-dimensional magnetotelluric inversion of blocky geoelectrical structures: Journal of Geophysical Research, **107**, doi:10.1029/2001JB000191.

Milkov, A. V., and R. Sassen, 2000, Thickness of the gas hydrate stability zone, Gulf of Mexico continental slope: Marine and Petroleum Geology, **17**, 981–991.

Newman, G. A., and D. L. Alumbaugh, 1995, Frequency-domain modelling of airborne electromagnetic responses using staggered finite differences: Geophysical Prospecting, **43**, 1021–1042.

———, 2000, Three-dimensional magnetotelluric inversion using nonlinear conjugate gradients: Geophysical Journal International, **140**, 410–424.

Ogilvie, J. S., and G. W. Purnell, 1996, Effects of salt-related mode conversions on subsalt prospecting: Geophysics, **61**, 331–348.

Park, S. K., and R. L. Mackie, 2000, Resistive (dry?) lower crust in an active orogen, Nanga Parbat, northern Pakistan: Tectonophysics, **316**, 359–380.

Peel, F. J., C. J. Travis, and J. R. Hossack, 1995, Genetic structural provinces and salt tectonics of the Cenozoic offshore U.S. Gulf of Mexico: A preliminary analysis, *in* M. P. A. Jackson, D. G. Roberts, and S. Snelson, eds., Salt tectonics: A global perspective: AAPG Memoir 65, 153–175.

Schuster, D. C., 1995, Deformation of allochthonous salt and evolution of related salt-structural systems, eastern Louisiana Gulf Coast, *in* M. P. A. Jackson, D. G. Roberts, and S. Snelson, eds., Salt tectonics: A global perspective: AAPG Memoir 65, 177–198.

Siripunvaraporn, W., G. Egbert, and M. Uyeshima, 2005, Interpretation of two-dimensional magnetotelluric profile data with three-dimensional inversion: Synthetic examples: Geophysical Journal International, **160**, no. 3, 804–814.

Smith, T., M. Hoversten, E. Gasperikova, and F. Morrison, 1999, Sharp boundary inversion of 2D magnetotelluric data: Geophysical Prospecting, **47**, 469–486.

Sternberg, B. K., J. C. Washburne, and L. Pellerin, 1988, Correction for static shifts in magnetotellurics using transient electromagnetic soundings: Geophysics, **53**, 1459–1468.

Vozoff, K., 1972, The magnetotelluric method in the exploration of sedimentary basins: Geophysics, **37**, 98–141.

Wannamaker, P. E., G. W. Hohmann, and S. H. Ward, 1984, Magnetotelluric responses of three-dimensional bodies in layered earths: Geophysics, **49**, 1517–1533.

Wannamaker, P. E., J. A. Stodt, and L. Rijo, 1987, A stable finite-element solution for two-dimensional magnetotelluric modeling: Geophysical Journal of the Royal Astronomical Society, **88**, 277–296.

Weiss, C. J., 2001, A matrix-free approach to solving the fully 3D electromagnetic induction problem: 71st Annual International Meeting, SEG, Expanded Abstracts, 1451–1454.